www.czasopisma.pan.pl PAN www.journals.pan.pl

ARCHIVES of FOUNDRY ENGINEERING

ISSN (2299-2944)
Volume 2020
Issue 2/2020

37 – 42

10.24425/afe.2020.131299

6/2

Published quarterly as the organ of the Foundry Commission of the Polish Academy of Sciences

Intermetallic Phases in Alloyed Cast Iron with 18%Si Addition

M. Stawarz
Silesian University of Technology, Department of Foundry Engineering,
7 Towarowa Str. 44-100 Gliwice, Poland
* Corresponding author. E-mail address: marcin.stawarz@polsl.pl

Received 02.10.2019; accepted in revised form 01.12.2019

Abstract

The paper presents an analysis of a selected grade of high silicon cast iron intended for work in corrosive and abrasive conditions. The text describes its microstructure taking into account the process of crystallization, TDA analysis, EDS, XRD and the chemical composition analysis. In order to determine the phase composition, X-ray diffraction tests were carried out. The tests were executed on a Panalytical X'Pert PRO X-ray diffractometer with filtration of radiation from a lamp with copper anode and PIXcel 3D detector on the deflected beam axis. Completed tests allowed to describe the microstructure with detailed consideration of intermetallic phases present in the alloy. Results of the analysis of the examined alloy clearly show that we deal with intermetallic phases of Fe_3Si, Fe_5Si_3 types, as well as silicon ferrite and crystals of silicon. In the examined alloy, we observed the phenomenon of segregation of carbon, which, as a result of this process, enriches the surface of silicon crystals, not creating a compound with it. Moreover, the paper demonstrates capability for crystallization of spheroidal graphite in the examined alloy despite lack of elements that contribute to balling in the charge materials.

Keywords: Theory of crystallization, Solidification process, Intermetallic phases, Spheroidal graphite, Silicon cast iron

1. Introduction

According to the definition presented in the paper [1], the cast iron belongs to a group of multi-component technical iron and carbon alloys. To differentiate it from steel or steel casting, it is defined as a cast alloy of a carbon content that ensures solidification of the end liquid phase in eutectic temperature, and this content amounts to at least 2.08% in case of double Fe-C alloy. Cast iron, due to the fact that it contains other elements (Mn, P, S) and elements that are treated as alloys (Ni, Cr, Cu), may change the carbon content to a high extent.

The cast alloy described in the papers [2-5] confirms the aforementioned definition. Alloying elements [6-10] added to cast iron, apart from impacting the carbon content, also cause creation of phases [1-5] in the microstructure of the alloy, providing it with special parameters that allow to apply the analyzed alloy in specific work conditions [1, 3, 11-19]. The paper includes analysis of a alloy cast iron with addition of silicon above 18%.

2. Work methodology

The tests were carried out based on two-stage metallurgic processing of a liquid metal. Experimental melting was carried out in an induction furnace of medium frequency and capacity of 25 kg. Steel scrap of low sulphur content was used as a charge. Remaining components added during melting included: ferrosilicon FeSi75, synthetic graphite of carbon content above 99.35%. Steel scrap was appropriately prepared for each melting process by removal of oxides and other contaminations as well as degreased before the weighing process. Then, the scrap was dried in temperature of 250°C for 2h. A weighed portion of ferrosilicon FeSi75 was annealed in temperature of 650°C for 2h in a chamber furnace. Another stage included initial melting, which consisted in melting of steel scrap with addition of a graphite carburizer and ferrosilicon. The prepared and melted material, after removal of slug, was poured into steel casting mold. In the next step, the material prepared this way was used in proper melting. The

procedure of double melting aims to eliminate gas dissolved in liquid alloy [20-21]. During initial melting, samples for carbon content analysis were collected. The planned carbon content for the analyzed smelt was 0.5%.

The second stage of melting consisted in melting a charge that was previously prepared in an induction furnace and possible correction of the carbon content. During melting of the charge, the metal bath degassing method was applied [20]. It consisted in overheating of a melted metal to temperature of 1400˚C, and then gradual reduction of the temperature in the furnace to the value of approx. 1200˚C in order to remove gas from the bath [21]. After the liquid alloy reached temperature of 1200˚C, it was heated to temperature of approx. 1350˚C. Then, the liquid metal was poured into a ladle, the bottom of which was covered with FeTi67 foundry alloy in order to degas the metal bath. Metallographic examinations were conducted using scanning microscopy (Phenom Pro-X scanning microscope including EDS system) and Nikon Eclipse LV150N light microscope. Non-etched metallographic specimen were used in the examinations. Metallographic specimens were cut from samples in which thermal elements were placed during ATD analysis.

Station for registration of temperature changes in time was composed of ATD-S sampler (placed in a metal molding box made of molding mass composed of quartz sand and bentonite) with S type thermal element (Pt-PtRh 10) located in the measuring part in a quartz cover. Compensating cables were connected to a multi-channel transducer (Crystaldigraph M24). A signal from the multi-channel transducer was sent using RS323 connector to a mobile computer equipped with software for registration of temperature changes over time.

In order to determine the phase composition, X-ray diffraction tests were carried out. The tests were executed on a Panalytical X'Pert PRO X-ray diffractometer with filtration of radiation from a lamp with copper anode and PIXcel 3D detector on the deflected beam axis. The measurement was carried out using a stepwise method. Measurement parameters: angle range: from 20 to 120 degrees 2Θ, step: 0.026 degree, scanning time, step: 100s, average “K alpha” wave length for a cobalt lamp: 1.7909 A (0.179 nm).

3. Research results

3.1. Chemical composition analysis

The chemical composition analysis was conducted using Leco GDS 500 spectrometer and Leco Carbon-Sulphur Determinator CS125. The Si content analysis based on a weighing method was conducted in the Chemical Analyzes Laboratory of the Institute of Welding in Gliwice. The results of the aforementioned analyzes are presented in Table 1.

Table 1.
Chemical composition of the tested high silicon cast iron

Element content, % wt.								
**Si	*C	*S	P	Mn	Mo	Cu	Mg	Ti
18.70	0.52	0.003	0.022	0.301	0.022	0.064	0.00	0.027

*CS 125 Leco carbon and sulfur analysis,
** Si analysis using the weighing method

3.2. TDA analysis

Heating effect from the secondary crystallization process (Fe_2Si phase change into Fe_5Si_3 phase) for the temperature range of 1000-1030°C was noticed in the analyzed case. This effect was marked blue in the figure 1.

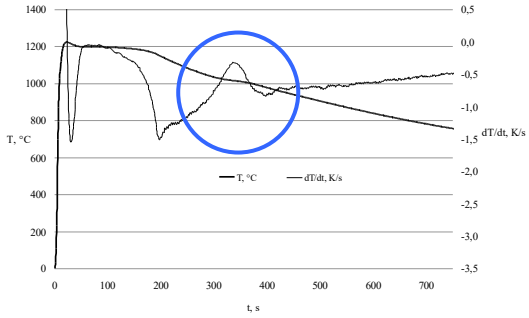

Fig. 1. Changes of temperature over time for the high silicon alloy cast iron of Si content at the level of 18.7%

3.3. SEM analysis

Fig. 2 presents the results of the metallographic analysis of the examined alloy. Elements decomposition maps (Fe, Si) are presented for the selected fragment of the sample.

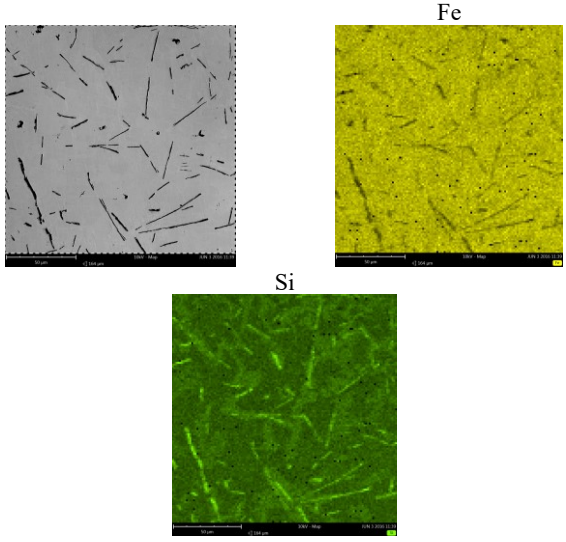

Fig. 2. Cast iron microstructure with visible Fe_3Si intermetallic phase separation. Elements decomposition maps

The linear analysis via separation of primary phase Fe_3Si (black needle-shaped separation) and the secondary phase Fe_5Si_3 that surrounds it (a gray area that surrounds the black primary needle-shaped separation) is presented in fig. 3. A close correlation for the iron and silicon content is visible.

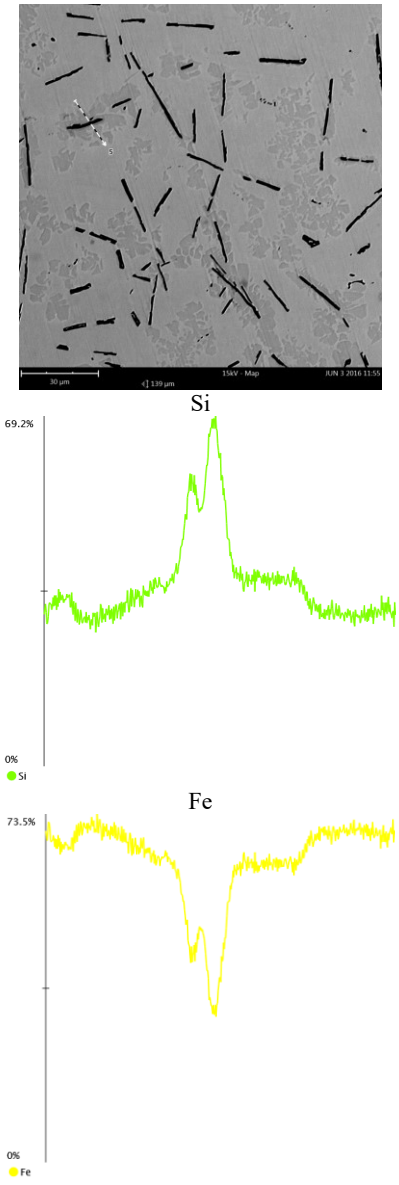

Fig. 3. The cast iron microstructure with visible intermetallic phase separation. Linear decomposition of iron and silicon

The following is an analysis of separation of a crystalline silicon, placed centrally in the figure (fig. 4) and surrounded by a bright silicon ferrite, darker intermetallic phase Fe_5Si_3 and black needles of the primary intermetallic phase of Fe_3Si type. There is a bright area in the centre of the crystalline silicon (fig. 4). EDS analysis does not allow to clearly answer the question regarding the type of internal silicon separation we observe with in this case. We do not know whether this is a silicon ferrite or a intermetallic phase.

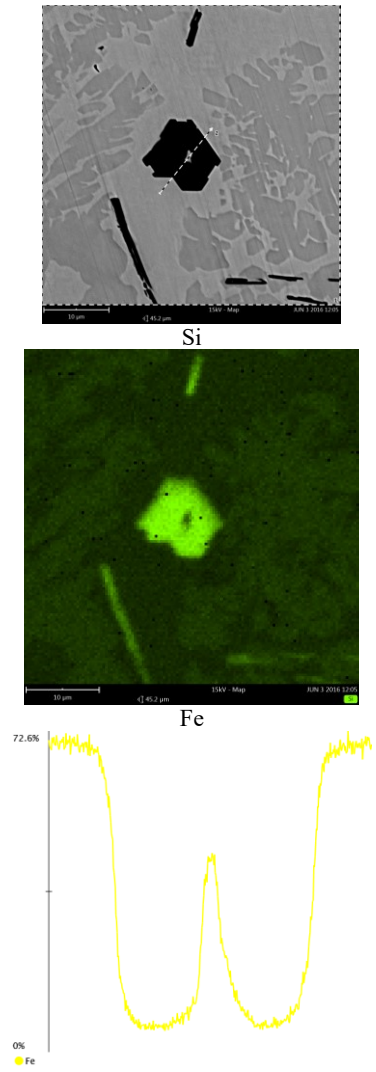

Fig. 4. The cast iron microstructure with visible, central separation of silicon. The elements decomposition maps including linear decomposition of iron, silicon and carbon [22]

The next stage of tests included EDS analysis in order to recognise the surface of the contraction cavity observed in the tested sample. Separations of nodular graphite, single or accumulated in clusters, were observed on the surface of the contraction cavity. The probable cause of presence of nodular graphite is small sulfur content in charge materials used in melting. Example spheroidal separation is presented in fig. 5 including EDS analysis.

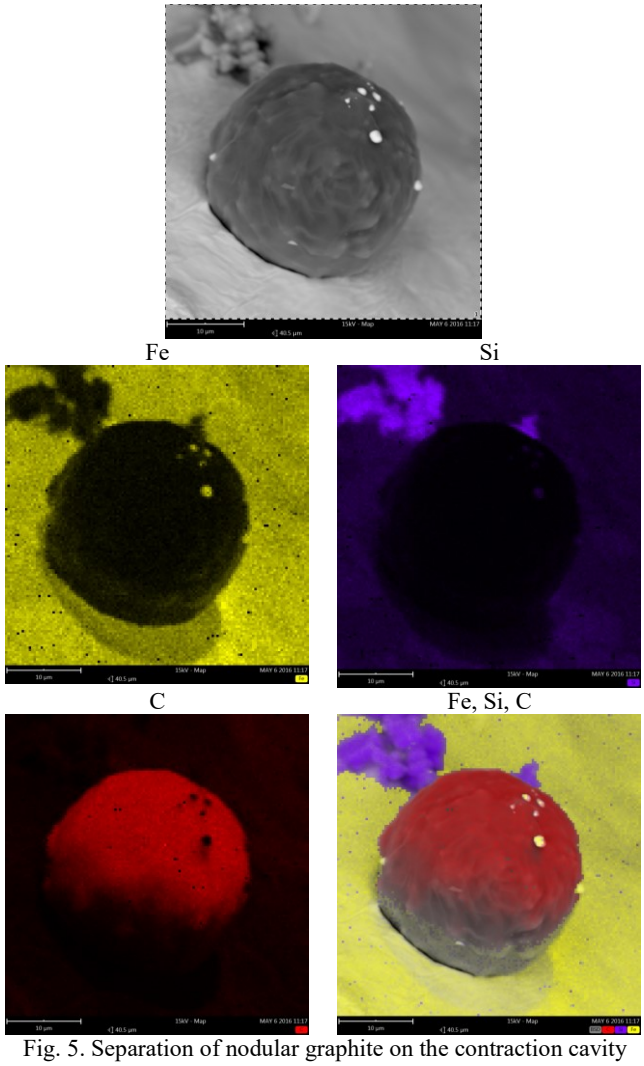

Fig. 5. Separation of nodular graphite on the contraction cavity surface. Elements decomposition maps [22]

3.4. XRD analysis

Results of the analysis of the examined alloy (fig. 6) clearly show that we deal with intermetallic phases of Fe_3Si, Fe_5Si_3 types, as well as silicon ferrite.

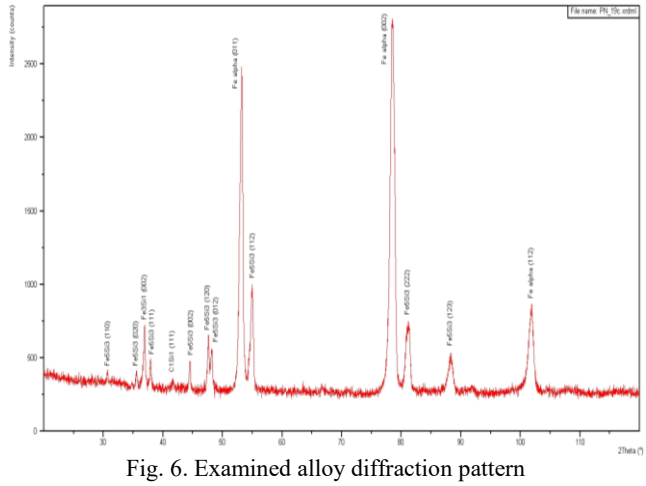

Fig. 6. Examined alloy diffraction pattern

In the examined alloy, we observe the phenomenon of segregation of carbon, which, as a result of this process, enriches the surface of silicon crystals, not creating a compound with it. The temperature of formation of SiC compound [23-24], as well as the conditions in which such compounds are formed, significantly deviate from the conditions and the temperature range that cause crystallization of the alloy. On the other hand, the author of the book [1] states that addition of ferrosilicon of increased Si content to the alloy causes formation of areas saturated with silicon, while the diffusion of carbon atoms causes formation of carbon-enriched areas on the borders of silicon-enriched areas. In the further part of the work [1], the author states that contact between silicon-enriched (FeSi) and carbon-enriched (Fe_3C) areas may lead to reaction $Fe_3C + FeSi = SiC + 4Fe$, which results in formation of silicon carbide, which is then dissolved by iron. In the other fragment of the work [1], the author suggests that the increase of silicon content is accompanied by narrowing of the range of occurrence of γ phase. Silicon freely dissolves in a liquid state, while in solid state it mainly dissolves in ferrite (up to 15% in room temperature and up to 18.5% in temperature of 1040°C). At increased Si content (above 16%), a triple eutectic is formed: Si solution in ferrite – graphite – FeSi. In case of coagulation according to metastable system for increased Si content (approximately 22%), SiC silicon carbide appears [1].

4. Conclusions

It was observed that an increased silicon additive added to the alloy and reduced sulphur content create conditions for intrinsic crystallization of nodular graphite without participation of elements that contribute to graphite balling.

The structure of the surface layer of graphite separations observed in the surface of the contraction cavity suggests that this is a primary graphite that crystallizes in a metal liquid, which is confirmed by authors in the papers [25-30].

The results of X-ray analysis clearly show that the examined alloy contains intermetallic phases of Fe_3Si, Fe_5Si_3 types, as well as silicon ferrite.

Due to increased silicon content in the alloy, the solubility of carbon, the atoms of which are transported before the

crystallization front, is significantly reduced. This phenomenon is documented in a form of spheroidal graphite separations on the surface of the contraction cavities, as well as an increased carbon content in an unstructured form on the surface of the contraction cavities.

Acknowledgements

This publication was financed from the statutory subsidy of the Faculty of Mechanical Engineering of the Silesian University of Technology in 2019.

References

[1] Podrzucki, C. (1991). *Cast Iron*. Volume 1&2. Kraków: ZG Stop. (in Polish).
[2] Fraś, E. & Podrzucki, C. (1981). *Modified cast iron.* Volume 675. Kraków: AGH. (in Polish).
[3] Kosowski, A. & Podrzucki, C. (1981). *Alloy cast iron.* Volume 825. Kraków AGH. (in Polish).
[4] Sakwa, W. (1974). *Cast Iron*. Śląsk: Katowice. (in Polish).
[5] Edited by Davis, J.R. (1996). *Cast Irons*,, ASM International. Handbook Committee, Materials Park, Ohio, ASM International.
[6] EL-Sawy, E.E.T., El-Hebeary, M.R. & El Mahallawi, I.S.E. (2017). Effect of manganese, silicon and chromium additions on microstructure and wear characteristics of grey cast iron for sugar industries applications. *Wear*. 390-391, 113-124. https://doi.org/10.1016/j.wear.2017.07.007.
[7] Johnson, O., Talabi, S. I., Olumuyiwa, I. A. & Afemefuna, T. O. (2013). Effect of silicon additions on the wear properties of grey cast iron. *Journal of Minerals and Materials Characterization and Engineering*. 1, 61-67. DOI:10.4236/jmmce.2013.12012.
[8] Mohamed, I.A., Ibraheem, A.A., Khashaba, M.I. & Ali, W. (2013). Influence of heat treatment on friction and wear of ductile iron: role of copper and molybdenum. *International Journal of Control, Automation and Systems*. 2(3), 23-30.
[9] Atanda, P., Okeowo, A. & Oluwole, O. (2010). Microstructural study of heat treated chromium alloyed grey cast iron. *Journal of Materials Engineering and Performance.* 9(3), 263-274. DOI: 10.4236/jmmce.2010.93021.
[10] Agunsoye, O., Bello, S. A., Hassan, S. B., Adeyemo, R. G. & Odii, J. M. (2014). The effect of copper addition on the mechanical and wear properties of grey cast iron. *Journal of Minerals and Materials Characterization and Engineering*. 2, 470-483. DOI: 10.4236/jmmce.2014.25048.
[11] Delprete, C., Sesana, R. & Vercelli, A. (2010). Multiaxial damage assessment and life estimation: application to an automotive exhaust manifold. *Procedia Engineering*. 2, 725-734. DOI:10.1016/j.proeng.2010.03.078.
[12] Magnusson Åberg, L. & Hartung, C. (2012). Solidification of SiMo Nodular cast iron for high temperature applications. *Trans Indian Inst Met.* 65(6), 633-636. DOI 10.1007/s12666-012-0216-8.
[13] Matteis, P. Scavino, G., Castello, A. & Firrao, D. (2014,). High temperature fatigue properties of a Si-Mo ductile cast iron. *Procedia Materials Science* 3, 2154-2159. DOI: 10.1016/j.mspro.2014.06.349.
[14] Korb, L. J. & Olson, D. L. (1992). *Corrosion*. Volume 13, (9th ed.), International ASM Handbook.
[15] Stefanescu, D.M. (1998). *Casting.* Volume 15. (4th ed.). International ASM Handbook.
[16] Wojciechowski, Ł., Eymard, S., Ignaszak, Z. & Mathia, T.G. (2015). Fundamentals of ductile cast iron scuffing at the boundary lubrication regime. *Tribology International*. 90, 445-454.
[17] Li, J., Wang, S., Zhao, A., Wang, L. & Liu, F. (2007). Corrosion properties of high silicon iron-based alloys in nitric acid. *China Foundry*. 4(4), 276-279.
[18] Kim, B.H., Shin, J.S., Lee, S.M. & Moon, B.M. (2007). Improvement of tensile strength and corrosion resistance of high-silicon cast irons by optimizing casting process parameters. *Journal of Materials Science*. 42, 109-117. DOI 10.1007/s10853-006-1081-9.
[19] Castro, D.B.V., Rossini, L.S., Malafaia, A.M.S., Angeloni, M. & Maluf, O. (2011). Influence of Annealing Heat Treatment and Cr, Mg, and Ti Alloying on the Mechanical Properties of High-Silicon Cast Iron, *Journal of Materials Engineering and Performance.* 20(7), 1346-1354. DOI: 10.1007/s11665-010-9733-y
[20] Stawarz, M., Gromczyk, M., Jezierski, J. & Janerka, K. (2015). Analysis of the high silicon cast iron crystallization process with TDA method. In Metal 2015: 24th International Conference on Metallurgy and Materials. Ostrava: TANGER 2015, (pp. 42-47).
[21] Stawarz, M., Janerka, K., Jezierski, J. & Szajnar, J. (2014). Thermal effect of phase transformations in high silicon cast iron. In Metal 2014: 23rd International Conference on Metallurgy and Materials. Ostrava: TANGER 2014, (pp.123-128).
[22] Stawarz, M. (2019). *The role of intermetallic phases in silicon cast iron.* Katowice - Gliwice: Archives of Foundry Engineering. (in Polish).
[23] Onsoien, M. I. & Skaland, T. (2001). *Preconditioning of Gray Iron Melts using Ferrosilicon or Silicon Carbon*, American Foundry Society.
[24] Janerka, K. (2010): *Carburizing of liquid iron alloys*. Gliwice: Silesian Technical University. (in Polish).
[25] Stefanescu, D.M., Alonso, G., Larranaga, P., De la Fuente, E. & Suarez, R. (2016). On the crystallization of graphite from liquid iron - carbon – silicon melts. *Acta Materialia*. 107, 102-126. DOI: 10.1016/j.actamat.2016.01.047.
[26] Stefanescu, D.M., Alonso, G., Larranaga, P., De la Fuente, E. & Suarez, R. (2017). Reexamination of crystal growth theory of graphite in iron-carbon alloys. *Acta Materialia*. 139, 109 – 121. DOI: 10.1016/j.actamat.2017.08.004.
[27] Stefanescu, D.M., Alonso, G., Larranaga, P., De la Fuente, E. & Suarez R. (2018). Reassessment of crystal growth theory of graphite in cast iron. *Materials Science Forum*. 925, 36-44. DOI: 10.4028/www.scientific.net/MSF.925.36.
[28] Alonso, G., Stefanescu, D.M., De la Fuente, E., Larranaga, P. & Suarez, R. (2018). The influence of trace elements on the nature of the nuclei of the graphite in ductile iron. *Materials*

Science Forum. 925, 78-85. DOI: 10.4028/www.scientific.net/MSF.925.78.

[29] Górny, M. & Stefanescu, D.M. (2017). Thin-wall ductile iron castings. In Cast Iron Science and Technology. Stefanescu, D.M., Ed.; ASM Handbook; ASM International: Columbus, OH, USA; Volume 1A, 617-628, ISBN 978-1-62708-133-7.

[30] Górny, M., Kawalec, M., Sikora, G., Olejnik, E., & Lopez, H. (2018). Primary Structure and Graphite Nodules in Thin-Walled High-Nickel Ductile Iron Castings. *Metals.* 8, 649. DOI:10.3390/met8080649.